Fast electrons from collisions of highly stripped ions with solid-state targets

D. H. Jakubassa-Amundsen[1] and H. Rothard[2]
[1]*Physics Section, University of Munich, 85748 Garching, Germany*
[2]*Centre Interdisciplinaire de Recherches Ions Lasers, CIRIL-GANIL (CEA/CNRS UMR 6632/ISMRA), Rue Claude Bloch, Boîte Postale 5133, 14070 Caen Cedex 05, France*
(Received 19 October 1998)

The momentum distribution of fast binary-encounter electrons emitted from solid-state targets of various thicknesses is investigated both theoretically and experimentally. The production of electrons in binary-type collisions with fast, highly stripped ions is calculated in the electron-impact approximation. A transport theory is formulated which allows for energy loss as well as angular deflection of the electrons (within the separation of energy loss and angular scattering approximation) during penetration of the target. The broadening of the binary encounter peak with increasing target thickness observed experimentally in 13.6-MeV/u Ar^{17+} and Ar^{18+} colliding with carbon foils is well described by theory. [S1050-2947(99)00907-5]

PACS number(s): 34.50.Fa, 78.70.−g, 79.20.Ap, 34.80.−i

I. INTRODUCTION

In fast ion-atom collisions, high-energy electrons are ejected from the target atoms in a binary-type interaction with the projectile ion. The momentum distribution of these electrons shows the typical binary ridge, being centered around an energy $E_0=2v^2\cos^2\vartheta$ for emission angles $\vartheta<90°$, where v is the collision velocity. In the case of solid-state targets, this momentum distribution is modified because the electrons undergo multiple collisions with target atoms when penetrating the target. The development of multiple-scattering theories for elastic and inelastic collisions dates back to Goudsmit and Saunderson [1] and Landau [2], respectively. Electron scattering from the target cores, being basically elastic, leads to angular deflection, while the scattering from the target valence electrons is an inelastic process resulting in energy loss. If the velocity of the heavy-ion-induced electrons is considerably larger than typical intrinsic velocities of the target electrons, these two processes can be treated separately [the so-called SELAS (separation of energy loss and angular scattering) approximation [3,4]]. This approximation, in combination with a multiple-scattering expansion for the penetrating electrons, was recently applied for a detailed comparison with experimental data [5].

Experiments using a monoenergetic electron beam impinging on a solid target [5,6] considered predominantly the stopping power or angular deflection of the penetrating electrons. Instead of an electron beam, convoy electrons created inside the target and traveling with the positively charged projectiles were also studied, and their integral yields [7] or energy distribution [8] behind the target were measured.

Experiments relying on the binary encounter mechanism for the production of fast electrons [4,9–11] have the advantage that they allow for a simultaneous investigation of electron penetration in different directions, which is of particular interest for inhomogeneous media. A measurement of the doubly differential cross section for electron emission behind the foil shows the influence of solid-state effects both on the spectra and the angular distributions. Such experiments were recently carried out using foils of varying thickness [12]. Also, the electron velocity was extended to the relativistic regime [13,14].

Up to now the thus measured electronic momentum distributions have only been compared with Monte Carlo calculations [9,10], or with a quantum-mechanical single-collision theory which neglects electron transport effects [14,15]. For thicker targets, the calculations are at variance with experiment, providing binary encounter peak widths which are far too small, particularly at the larger emission angles.

In this work a theory is developed which combines an accurate description of the electron production by means of electron capture to the projectile continuum with a transport theory allowing for energy loss and angular straggling of these electrons when penetrating the target. This is an improvement over earlier simple models [16] for binary encounter electron transmission. A relativistic formulation of the theory is given in Sec. II, and results for 13.6-MeV/u Ar^{18+}+C are shown in Sec. III. The experiments with Ar^{17+} as well as Ar^{18+} projectiles colliding with carbon foils of thickness up to 356 $\mu g/cm^2$ are described in Sec. IV and the measured spectra are compared with theory. The conclusion is drawn in Sec. V. Atomic units ($\hbar=m=e=1$) are used unless otherwise indicated.

II. TRANSPORT THEORY

When electrons are created at a certain distance x' behind the entrance surface (see Fig. 1), they are slowed down and deflected on their way through the target before reaching the detector behind the exit surface at x. Since fast electrons are

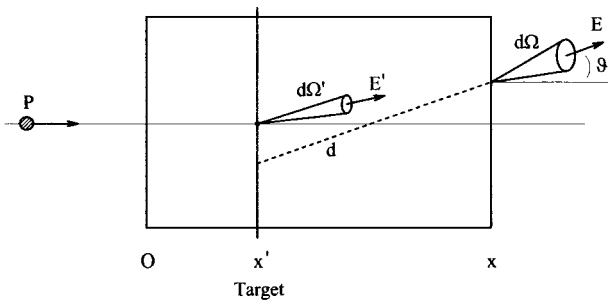

FIG. 1. Schematic view of a projectile P impinging on a solid target of thickness x.

predominantly emitted into forward directions and suffer mostly small-angle deflections, any backward scattering during their penetration from x' to x will be neglected. The momentum distribution of the detected electrons is obtained by folding the production cross section $d^2\sigma/dE'd\Omega'$ with the distribution function f which gives the probability that an electron created at x' with energy E', originally emitted into the solid angle $d\Omega'$, has acquired an energy E and is ejected into $d\Omega$ at the target exit surface x. Hence, the electron yield behind the target is obtained from

$$\frac{d^2Y}{dEd\Omega}=\int_0^x dx'\int_{E_{\min}}^{E_{\max}}dE'\int d\Omega' \times\frac{d^2\sigma}{dE'd\Omega'}(E',\vartheta')\ \ f(E',E,\Omega',\Omega,x',x). \tag{2.1}$$

The production cross section is calculated in the relativistic electron-impact approximation (EIA), a first-order theory which describes target ionization by means of electron capture to the projectile continuum. This theory is well suited for the ejection of valence electrons by heavy, highly stripped projectiles, as it treats the projectile field nonperturbatively. One obtains[1] [15]

$$\frac{d^2\sigma}{dE_fd\Omega_f}(E_f,\vartheta_f)=\frac{k_fE_f}{vc^2}\sum_i\int d\vec{q}\,\delta(E_f^P-E_i^T\gamma+q_z\gamma v)\,\gamma_p^{-2} \times\frac{d\sigma_e^{\rm rel}(p,\vartheta_p)}{d\Omega}|\varphi_i^T(\vec{q})|^2, \tag{2.2}$$

where E_f and E_f^P is the emission energy of the electron in the target and projectile frame of reference, respectively, $\gamma=(1-v^2/c^2)^{-1/2}$ is the Lorentz factor, and E_i^T is the energy of the initial target state. Basically, Eq. (2.2) results from folding the relativistic cross section $d\sigma_e^{\rm rel}/d\Omega$ for elastically scattering an electron from the projectile field, with the transverse momentum distribution φ_i^T of its initial state. [The prefactor N_i^T of the initial-state Darwin function is suppressed in Eq. (2.2); it is very close to unity for a carbon target.] When summed over all target electrons, the dependence of Eq. (2.2) on the longitudinal momentum component q_z is closely related to the target Compton profile. The quantities p, ϑ_p, and $\gamma_p=(1+p^2/c^2)^{1/2}$ are defined from an on-shell approximation [15], and the quantization axis $\vec{e}_z$ has been taken along $\vec{v}$.

The electronic distribution function can be obtained from solving the master equation [5]. However, for fast electrons and sufficiently thin targets such that $(E'-E)/E'\ll 1$ for all $E'>E$, f may be factorized into two distribution functions g and h, corresponding to a decoupling of energy loss and angular deflection [3–5]

$$f(E',E,\Omega',\Omega,x',x)=g(E',E,d)\ \ h(\overline{E},\theta,d). \tag{2.3}$$

This factorization relies on the fact that elastic scattering occurs basically in binary encounters with the target cores, permitting only angular deflection but no energy loss. On the other hand, in collisions with target valence electrons, the fast electrons are hardly deflected, but lose energy upon exciting or ionizing the target. These two kinds of collisions are thus independent.

The distribution function g for energy loss is given by [2,5]

$$g(E',E,d)=\frac{1}{2\pi}e^{-d/\lambda_{\rm in}}\int_{-\infty}^{\infty}dk\,e^{ik(E'-E)}e^{d\tilde{W}_1(k)}. \tag{2.4}$$

Here $\lambda_{\rm in}=(N\sigma^{(\rm in)})^{-1}$ is the mean free path for inelastic scattering related to the target density N and the cross section $\sigma^{(\rm in)}=(1/N)\int dT\,W_1(T)$, where $W_1(T)$ is the kernel for inelastic scattering with energy transfer $T=E'-E$, and $\tilde{W}_1(k)$ its Fourier transform. One can show that an expansion of the exponent $d\tilde{W}_1(k)$ of the Fourier coefficient in terms of k (retaining only the zeroth- and first-order term) leads to

$$g(E',E,d)=\delta(E'-E-\Delta E(d)), \tag{2.5}$$

with $\Delta E(d)=d\int dT\,W_1(T)T$, the mean energy loss on a path of length d. Approximation (2.5) is better justified the shorter the collision time during which a given energy transfer T takes place, i.e., the higher the energy E' of the electrons [3,4]. The energy loss of the electrons is described as a continuous slowing down, given by the energy-dependent stopping power $S(E')$. Hence, with the help of Eq. (2.5),

$$E'-E=\Delta E(d)=\int_0^d ds\,S(E'), \tag{2.6}$$

where the explicit dependence of $E'=E'(E,s)$ on the location $s=s(x')$ must be taken into consideration. For the stopping power, the relativistic Bethe formula is used, including the Bloch correction [17,18]

$$S(E')=\frac{4\pi}{v'^2}NZ_T\left[\ln\frac{2v'^2}{I}-\ln\left(1-\frac{v'^2}{c^2}\right)-\frac{v'^2}{c^2} +\psi(1)-{\rm Re}\,\psi\left(1+\frac{i}{v'}\right)\right], \tag{2.7}$$

with Z_T and I the target nuclear charge and mean excitation energy (approximated by the ionization threshold, $I=9$ eV for carbon), respectively. The velocity $v'=c(1-c^4/(E'+c^2)^2)^{1/2}$, and ψ is the psi function, Re ψ denoting its real part.

Into the distribution function $g(E',E,d)$ from Eq. (2.3) enters the actual path length d the electron has traveled when moving from x' to x. From Fig. 1 it is clear that only in case of zero scattering angle, d is equal to $x-x'$, but is larger otherwise. We include the ϑ dependence in a simple way [4]:

$$d=\frac{x-x'}{\cos\vartheta}. \tag{2.8}$$

[1] In Ref. [12], Eq. (4), $q_z\gamma$ should read $q_z\gamma v$ in the argument of the δ function.

Although strictly valid only for a straight-line path [3], this is a reasonable approximation for forward scattering, and superior to the choice of $d=x-x'$ used elsewhere [5].

The distribution function h in Eq. (2.3) for angular scattering is, in analogy to Eq. (2.4), given in terms of a basis state expansion [1,5]

$$h(\overline{E},\theta,d)=\frac{1}{4\pi}e^{-d/\lambda_{\rm el}}\sum_{l=0}^{\infty}(2l+1)P_l(\cos\theta)e^{d\tilde{W}_2(l)}, \tag{2.9}$$

where $\lambda_{\rm el}=(N\sigma^{(\rm el)})^{-1}$ is the mean free path for elastic scattering. $\tilde{W}_2(l)$ is the Legendre transform

$$\tilde{W}_2(l)=\int_{-1}^{1}d(\cos\theta)P_l(\cos\theta)W_2(\theta) \tag{2.10}$$

of the kernel $W_2(\theta)$ for elastic scattering with deflection by the angle θ. It is related to the cross section $\sigma^{(\rm el)}$ through $N\sigma^{(\rm el)}=\tilde{W}_2(0)$.

Assuming the target atoms to be represented by a simple screened potential, $V=Z_T\exp(-\alpha r)/r$ with screening constant $\alpha=1.13Z_T^{1/3}$, $W_2(\theta)$ is found to be [1]

$$\begin{aligned}W_2(\theta)&=2\pi N\frac{d\sigma^{(\rm el)}}{d\Omega}\\&=2\pi N\frac{Z_T^2}{4\overline{v}^4}\left(1-\frac{\overline{v}^2}{c^2}\right)\frac{1}{\left(\sin^2\frac{\theta}{2}+y_0'^2\right)^2},\\ y_0'&=\frac{\alpha}{2\overline{v}}\left(1-\frac{\overline{v}^2}{c^2}\right)^{1/2}\end{aligned} \tag{2.11}$$

$\overline{v}$ is related to the mean collision energy $\overline{E}$ in the same way as given below Eq. (2.7), with $\overline{E}$ taken as $(E+E')/2$.

In order to speed up convergence in the sum over l, the zeroth-order scattering term [i.e., the one where $\exp(d\tilde{W}_2(l))$ in Eq. (2.9) is replaced by unity] is separated [5]:

$$h(\overline{E},\theta,d)=\frac{1}{4\pi}e^{-d/\lambda_{\rm el}}\left\{2\delta(\cos\theta-1)+\sum_{l=0}^{\infty}(2l+1)P_l(\cos\theta)[e^{d\tilde{W}_2(l)}-1]\right\}. \tag{2.12}$$

This allows for a truncation of the sum at $l_{\max}=60$ for the present collision systems.

Upon insertion of Eq. (2.3) into Eq. (2.1), the integral over x' can be done by means of the delta function in Eq. (2.5)

$$\begin{aligned}&\int_0^x dx'\,\delta(E'-E-\Delta E(d))F(x')\\&\quad=F(\overline{x})\left|\frac{\partial}{\partial x'}\Delta E(d)\right|^{-1}\\&\quad=F(\overline{x})\left|\frac{\partial}{\partial d}\Delta E(d)\,\frac{\partial d}{\partial x'}\right|^{-1}\\&\quad=F(\overline{x})\left|\frac{\cos\vartheta}{S(E')}\right|,\end{aligned} \tag{2.13}$$

where $\Delta E(d)$ and $d(x')$ were taken from Eqs. (2.6) and (2.8), and F is an abbreviation for the remaining integrand. Hence, approximation (2.5) relates to a given energy E' a fixed location $x'=:\overline{x}$. Making use of the definition of the stopping power, $S(E)=-dE/ds$, one obtains x' as a function of E' by integrating $ds=-dE/S(E)$:

$$d=\frac{x-x'}{\cos\vartheta}=\int_E^{E'}\frac{dE''}{S(E'')}. \tag{2.14}$$

This leads to the following expression for the electron yield (2.1)

$$\begin{aligned}\frac{d^2Y}{dE\,d\Omega}&=\int_E^{E_{\max}}dE'\left|\frac{\cos\vartheta}{S(E')}\right|\\&\quad\times\int d(\cos\vartheta')d\varphi'\frac{d^2\sigma}{dE'd\Omega'}(E',\vartheta')\\&\quad\times h(\overline{E},\theta,d).\end{aligned} \tag{2.15}$$

Assuming that the electrons can only lose energy in inelastic collisions, we have $E'\geqslant E$, such that the lower limit of the energy integral is equal to E. The upper energy limit $E_{\max}$ is obtained from Eq. (2.14) for $x'=0$ [which is conveniently achieved by evaluating the integral in Eq. (2.14) for a grid of E' values, with $E_{\max}$ resulting from a subsequent interpolation at the given value $d(0)=x/\cos\vartheta$]. Upon insertion of Eq. (2.9) for h, the integration over φ' in Eq. (2.15) can also be performed analytically. To this aim the Legendre polynomial $P_l(\cos\theta)$ depending on the deflection angle θ, i.e., the angle between the directions given by $d\Omega$ and $d\Omega'$ (Fig. 1), has to be decomposed. In the following we shall assume a spherical symmetry of the target, such that there is no φ' dependence of the production cross section. Hence in the multiple-scattering contribution to h one has simply

$$\begin{aligned}\int_0^{2\pi}d\varphi'P_l(\cos\theta)&=\int_0^{2\pi}d\varphi'\frac{4\pi}{2l+1}\sum_{m=-l}^{l}Y_{lm}^*(\Omega)Y_{lm}(\Omega')\\&=2\pi P_l(\cos\vartheta)P_l(\cos\vartheta')\end{aligned} \tag{2.16}$$

because only the $m=0$ contribution survives, due to the orthogonality of the spherical harmonics Y_{lm}. In the zero-

scattering contribution to h, the whole angular integral can easily be carried out if the direction of Ω is taken as quantization axis

$$\int d\Omega'\,\delta(\cos\theta-1)F(\vartheta') = F(\vartheta)2\pi\int_{-1}^{1} d(\cos\theta)\,\delta(\cos\theta-1) = 2\pi F(\vartheta). \tag{2.17}$$

Again, F symbolizes the remaining integrand. Taking all these results into account, we finally obtain the doubly differential emission cross section (equal to the yield per target length) in the following form

$$\left(\frac{d^2\sigma}{dEd\Omega}\right)_x = \frac{|\cos\vartheta|}{x}\int_E^{E_{\max}} dE'\frac{1}{|S(E')|}e^{-d/\lambda_{el}} \times\left\{\frac{d^2\sigma}{dE'd\Omega'}(E',\vartheta)+\frac{1}{2}\sum_{l=0}^{\infty}(2l+1)P_l(\cos\vartheta) \times[e^{d\tilde{W}_2(l)}-1]\int_{-1}^{1} d(\cos\vartheta')P_l(\cos\vartheta') \times\frac{d^2\sigma}{dE'd\Omega'}(E',\vartheta')\right\}. \tag{2.18}$$

The calculation of $\tilde{W}_2(l)$, Eq. (2.10) with Eq. (2.11), is done recursively. We have

$$\tilde{W}_2(l) = N\frac{\pi Z_T^2}{2\overline{v^4}}\left(1-\frac{\overline{v^2}}{c^2}\right)I_l, \tag{2.19}$$

$$I_l := \int_0^{\pi}\sin\theta\,d\theta\,P_l(\cos\theta)\frac{1}{\left(\sin^2\frac{\theta}{2}+y_0'^2\right)^2} = 2\int_{y_0'^2}^{1+y_0'^2} dx\,P_l(\cos\theta)\frac{1}{x^2},$$

where x is substituted for the bracket in the denominator. Using the recursion relation for the Legendre polynomials, one arrives at a recursion for I_l

$$I_{l+1} = \frac{2l+1}{l+1}(1+2y_0'^2)I_l - \frac{l}{l+1}I_{l-1} - \frac{2(2l+1)}{l+1}S_l, \qquad l=0,1\ldots, \tag{2.20}$$

where $\cos\theta = 1+2y_0'^2-2x$ is used, and S_l is found from

$$S_l := 2\int_{y_0'^2}^{1+y_0'^2} dx\,P_l(\cos\theta)\frac{1}{x}, \tag{2.21}$$

$$S_{l+1} = \frac{2l+1}{l+1}(1+2y_0'^2)S_l - \frac{l}{l+1}S_{l-1} - 4\delta_{l0}, \qquad l=0,1\ldots.$$

The starting values are $S_{-1}=I_{-1}=0$ and

$$S_0 = 2\ln\frac{1+y_0'^2}{y_0'^2}, \quad I_0 = \frac{2}{y_0'^2}-\frac{2}{1+y_0'^2}. \tag{2.22}$$

With these, there are only two integrals to be performed numerically in the evaluation of Eq. (2.18) for predetermined production cross sections. These production cross sections have to be provided on a closely spaced grid of energies E' and angles ϑ'. For emission angles $\vartheta \leqslant 40°$ and not too low energies E, we found it sufficient to truncate the ϑ' integral at 60° for the present systems.

III. THEORETICAL RESULTS

The transport theory described above (which will be called ''solid-EIA'' theory in the following) has been applied to the 13.6-MeV/u Ar^{18+}+C collision system. At such a moderate collision velocity ($v \approx 23$), relativistic effects are perceptible as a slight kinematical shift of the binary encounter peak to higher energies, but hardly influence the transport properties.

Figure 2 shows the resulting electron spectra at 0°, 15°, and 30° for target thicknesses ranging from 4.4 to 356 μg/cm^2. In order to compare with single-collision conditions, we make use of the fact that the inelastic mean free path λ_{in} for fast electrons can be approximated by a simple power law [19]

$$\lambda_{in} \approx AE^n, \tag{3.1}$$

where the energy E of the electron is measured in eV, and λ_{in} in Å. For a carbon target and $E > 200$ eV, one has [19] $A = 0.097$ and $n = 0.81$. Usually the target thicknesses X are given in units Nx, where x is the target length introduced earlier,

$$X = Nx, \tag{3.2}$$

such that for the present carbon target with $N = 1.65$ g/cm^3 [11], $x = 1$ Å corresponds to $X = 1.65\times10^{-2}$ μg/cm^2. It should be noted that in theory Eq. (2.18), x also enters only in combination with the target density given by Eq. (3.2). With the help of the Avogadro constant [20], Nx can be expressed in atomic units

$$Nx = X[\mu\text{g/cm}^2] = X\frac{6.022\times10^{23}}{A}\left[\frac{10^{-6}}{\text{cm}^2}\right] = X\frac{16.88}{A}[\text{a.u.}], \tag{3.3}$$

where A is the atomic mass number ($A = 12$ for carbon).

Inserting $E = 2v^2\cos^2\vartheta/[1-(v^2/c^2)\cos^2\vartheta]$, the approximate position of the binary encounter peak maximum [15], into Eq. (3.1), one obtains $N\lambda_{in} = 6.74$ μg/cm^2 for $v = 23.09$ and $\vartheta = 0$. The mean free path λ_{el} for elastic scattering is much larger: at the zero-degree peak energy, from our theory we obtain $N\lambda_{el} = 18.3$ μg/cm^2. The total mean free path is therefore $N\lambda = N\lambda_{el}\lambda_{in}/(\lambda_{el}+\lambda_{in}) = 4.9$ μg/cm^2. This means that λ_{in} alone provides a correct estimate of the order of magnitude of the (total) mean free path in the energy region considered here. Hence, only for the thinnest target, single collision conditions are guaranteed.

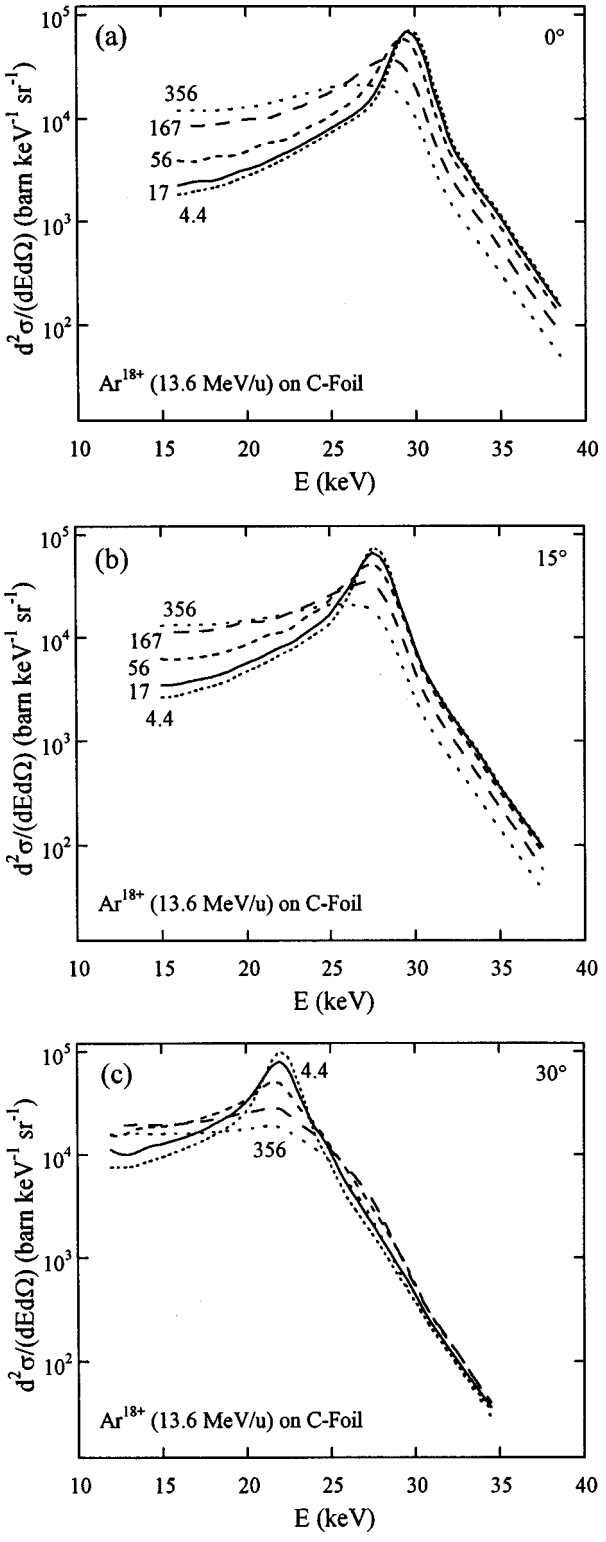

FIG. 2. Doubly differential electron emission cross section for 13.6-MeV/u Ar^{18+} impinging on C foils of thickness 4.4, 17, 56, 167, and 356 $\mu g/cm^2$ as a function of observation energy E. The emission angle is (a) 0°, (b) 15°, and (c) 30°.

From Fig. 2 a peak shift to lower energies as well as a broadening of the peak (combined with a decrease of the cross section) with increasing target thickness is visible, similarly to what was found for the velocity distribution of a monoenergetic electron beam measured behind a carbon foil [5]. The same features are found when the observation angle

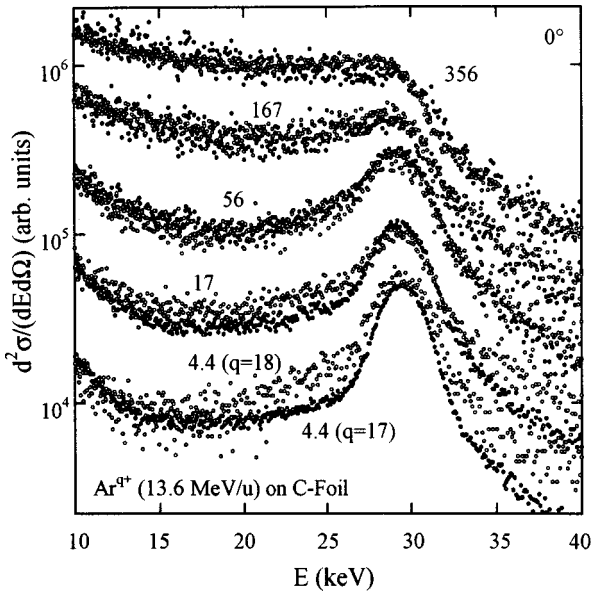

FIG. 3. Measured electron spectra (on a relative scale) at 0° from Ar^{17+} (●) and Ar^{18+} (○) impact on carbon targets of thickness ranging from 4.4 to 356 $\mu g/cm^2$.

is increased at a fixed target thickness. At 30°, the increase of the width with x is so strong that it leads to a crossover of the high-energy wings at medium-thick targets. This additional intensity results from the electrons which originally were emitted close to the beam direction (thus having a much higher energy and a similar intensity), but subsequently suffered angular deflections. A similar shoulder beyond the binary encounter peak was found in Monte Carlo calculations (and in experiment) for 3.5-MeV/u U^{38+} on carbon foils [9]. Only for the thickest target is this trend counterbalanced by the strong energy loss.

IV. EXPERIMENT IN COMPARISON WITH THEORY

The experiments were performed at the heavy-ion accelerator in Caen (France) in standard vacuum ($p < 10^{-6}$ mbar) with Ar^{17+} and Ar^{18+} projectiles of 13.6 MeV/u. Doubly differential electron spectra $d^2\sigma/dp\,d\Omega$ were recorded in the forward direction on the beam exit side of the foils at $\vartheta = 0°$ with perpendicular ion impact with the help of a magnetic analyzer. The angular acceptance was $\Delta\Omega \approx 2\times10^{-3}$, and the energy resolution[2] was $\Delta E/E \approx 0.05$. This corresponds to a momentum resolution $\Delta p/p \approx 0.024$ which was estimated from a more detailed analysis of the cusp width in the zero-degree spectra from Ref. [12]. Thin carbon foil targets produced by standard evaporation techniques were used. Their thickness was measured by techniques based on Rutherford scattering and energy-loss measurements. Further details can be found in Ref. [12].

Measurements at different emission angles (0°–180°) were only carried out for the thinnest target, using Ar^{17+} projectiles. Figure 3 gives a comparison of the 0° spectra resulting from Ar^{17+} and Ar^{18+} impact. It is evident that both

[2]In Ref. [12], the estimated experimental resolution should read $\Delta E/E \approx 0.05$ instead of $\Delta p/p \approx 0.05$.

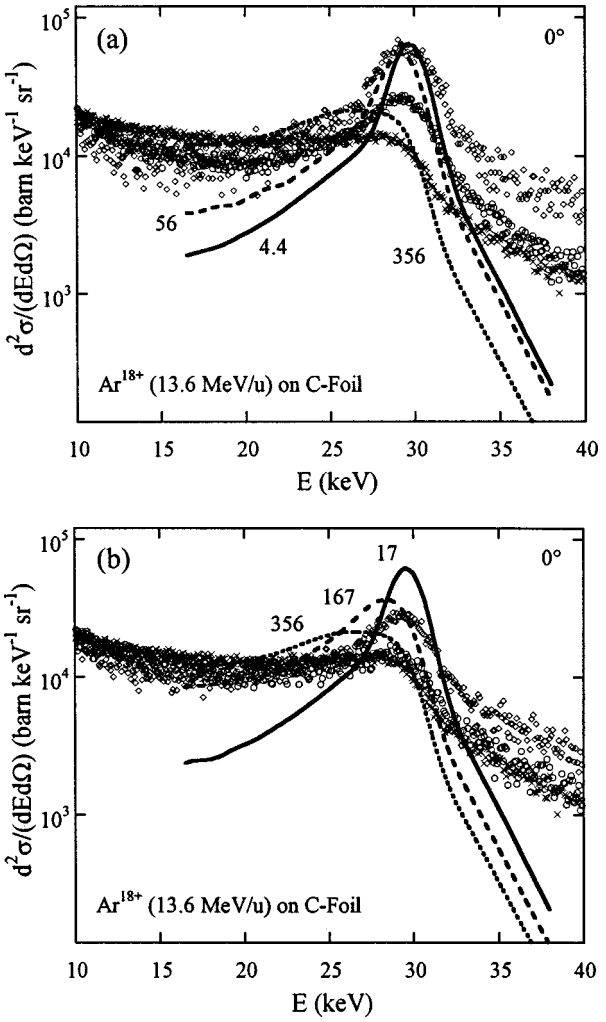

FIG. 4. Doubly differential electron emission cross section at 0° for 13.6-MeV/u Ar^{18+} impinging on C foils. (a) $X=4.4$, 56, and 356 $\mu g/cm^2$. (b) $X=17$, 167, and 356 $\mu g/cm^2$. ◇, experiment; —, theory for $X=4.4$ and 17 $\mu g/cm^2$; ○, experiment; - - -, theory for $X=56$ and 167 $\mu g/cm^2$; ×, experiment; ---, theory for 356 $\mu g/cm^2$.

sets of spectra agree mostly within the experimental uncertainty (15%) in the binary encounter peak region, irrespective of the foil thickness. From this we conjecture that the angular dependence of the electron yield will also be roughly the same for both kinds of projectiles. The same is true for the calculations, which only differ by about 5% when Ar^{18+} is changed to Ar^{17+} (the latter being much more time consuming; however, electron loss from Ar^{17+}, which is only important near the cusp, was not considered in the theory).

Figure 4 shows the doubly differential cross section from Ar^{18+} impact at $\vartheta=0$ for target thicknesses between 4.4 and 356 $\mu g/cm^2$. The theoretical curves from Fig. 2 were averaged over the detector momentum resolution (2.4%). Since the experimental spectra were only measured on a relative scale, they have been normalized to theory (i.e., the 0° spectrum for Ar^{18+} impact on 4.4-$\mu g/cm^2$ C was adjusted to the solid-EIA theory in the binary encounter peak maximum; this provides the normalization for all other Ar spectra). Also, the experimental energy scale was adjusted [12] to make the peak position coincide with theory for the thinnest target. It can be seen that the experimental intensity drops

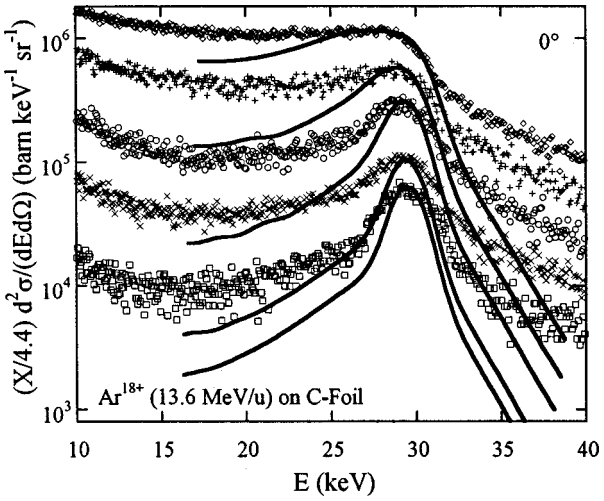

FIG. 5. Same spectra as in Fig. 4, with the experimental intensity scaled by $X/4.4$. Each calculated spectrum is now shifted both in energy and intensity to make the peak position and yield coincide with the corresponding measured spectra. (The target thickness increases from bottom to top.)

more strongly with X than predicted by theory. On the other hand, the peak shift is slightly overestimated by theory.

In order to compare the peak shapes, in Fig. 5 we have shifted the theoretical peak positions to make them agree with the experimental ones for all X, and also adjusted the peak intensities. The corresponding yields (equal to the cross-section times X) are shown at $\vartheta=0$, and although the calculated peak widths are in general too small, their increase with target thickness agrees well with the measurements. The difference between experiment and theory on the outermost wings of the peak may be due to energy straggling [10] (which is neglected in the present theory) or to background effects.

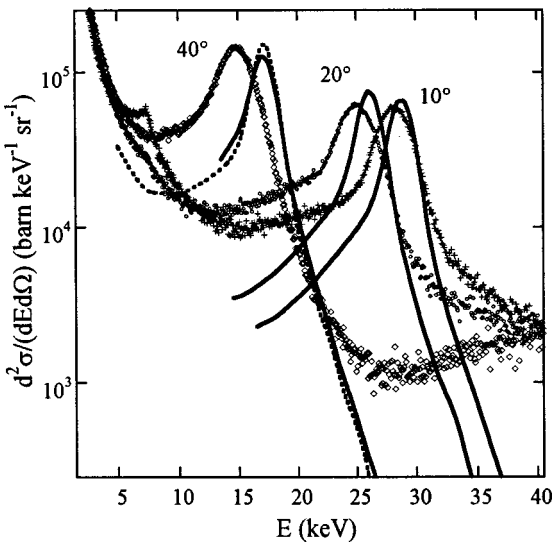

FIG. 6. Doubly differential electron emission cross section for 13.6-MeV/u Ar^{17+} (experiment) and Ar^{18+} (theory) impact on a 4.4-$\mu g/cm^2$ carbon foil at emission angles 10° (+), 20° (○), and 40° (◇). The solid lines give the solid-EIA results, and the broken line denotes the EIA result for 40°. The structure near 7.4 keV in the 10° data is the cusp from capture and loss to the projectile continuum.

Figure 6 shows the spectra at $X = 4.4\ \mu g/cm^2$ for emission angles between 10° and 40°. We have compared the data for Ar^{17+} impact with the theory for Ar^{18+} (in this figure only, we normalized the Ar^{17+} 0° spectrum for the thinnest target to the Ar^{18+} solid-EIA theory). It is seen that the peak intensities and shapes are fairly well reproduced by theory but the peak positions are not. In this context we recall that at an angle as large as 40°, the effective target length d [cf. Eq. (2.8)] is only 1.45 times the mean free path [12] such that even at the largest angle considered, solid-state effects should not be too important. The deviation between EIA [Eq. (2.2)] and solid-EIA results is indeed quite small (see Fig. 6).

V. CONCLUSION

We have measured doubly differential cross sections for binary encounter electron emission from carbon targets, systematically varying the foil thickness, and compared them with results from a quantum-mechanical high-energy transport theory. Both experiment and theory show an increase of the binary encounter peak width and a decrease of its intensity, as well as a peak shift to lower energies with increasing target thickness. However, while the width is in fair accord with the data, the peak intensity as well as the peak shift is overpredicted by theory.

In this context it should be noted that the SELAS approximation, i.e., the neglect of an interplay between elastic and inelastic collisions, is a rather crude approximation for the thicker targets, as has been observed previously [5]. Moreover, quite simple models were used both for the stopping power and for the kernel of the angular scattering, aiming at a qualitative agreement with experiment rather than at a quantitative one.

A still open question is the angular dependence of the binary encounter peak. Unfortunately, only data for the thinnest target are available where, according to theory, solid-state effects should be small for angles $\leqslant 40°$. Nevertheless, the present experiment shows a very strong peak shift as compared to the single-collision EIA theory, particularly at 40°, but surprisingly, again quite a small shift at 60° [12]. A similar anomaly at 40° is also present in the 77-MeV/u Ar^{18+}+Al data recorded for a larger target thickness [14]. The reason for this anomaly is presently not understood.

ACKNOWLEDGMENTS

It is a pleasure to thank the group of K. O. Groeneveld at the IKF, Frankfurt for stimulating the theory part of this work, and for the great hospitality we received during our numerous visits at the IKF. We would also like to thank G. Lanzanò, B. Gervais, and M. Beuve for important discussions.

[1] S. Goudsmit and J. L. Saunderson, Phys. Rev. **57**, 24 (1940).
[2] L. Landau, J. Phys. (Moscow) **8**, 1 (1944).
[3] S. Tougaard and P. Sigmund, Phys. Rev. B **25**, 4452 (1982).
[4] G. Schiwietz, J. P. Biersack, D. Schneider, N. Stolterfoht, D. Fink, V. J. Montemayor, and B. Skogvall, Phys. Rev. B **41**, 6262 (1990).
[5] S. Lencinas, J. Burgdörfer, J. Kemmler, O. Heil, K. Kroneberger, N. Keller, H. Rothard and K. O. Groeneveld, Phys. Rev. A **41**, 1435 (1990).
[6] V. E. Cosslett and R. N. Thomas, Br. J. Appl. Phys. **15**, 883 (1964); **15**, 1283 (1964).
[7] H. P. Hülskötter, J. Burgdörfer, and I. A. Sellin, Nucl. Instrum. Methods Phys. Res. B **24/25**, 147 (1987).
[8] P. Koschar, A. Clouvas, O. Heil, M. Burkhard, J. Kemmler, and K. O. Groeneveld, Nucl. Instrum. Methods Phys. Res. B **24/25**, 153 (1987).
[9] R. A. Sparrow, R. E. Olson, and D. Schneider, J. Phys. B **25**, L295 (1992).
[10] R. A. Sparrow, R. E. Olson, and D. Schneider, J. Phys. B **28**, 3427 (1995).
[11] H. Rothard, C. Caraby, A. Cassimi, B. Gervais, J.-P. Grandin, P. Jardin, M. Jung, A. Billebaud, M. Chevallier, K. O. Groeneveld, and R. Maier, Phys. Rev. A **51**, 3066 (1995).
[12] H. Rothard, D. H. Jakubassa-Amundsen, and A. Billebaud, J. Phys. B **31**, 1563 (1998).
[13] B. D. DePaola, Y. Kanai, P. Richard, Y. Nakai, T. Kambara, T. M. Kojima, and Y. Awaya, J. Phys. B **28**, 4283 (1995).
[14] G. Lanzanò, E. DeFilippo, S. Aiello, M. Geraci, A. Pagano, G. Politi, Sl. Cavallaro, F. Lo Piano, E. C. Pollaco, C. Volant, S. Vuillier, C. Beck, D. Mahboub, R. Nouicer, H. Rothard, and D. H. Jakubassa-Amundsen, Phys. Rev. A **58**, 3634 (1998).
[15] D. H. Jakubassa-Amundsen, J. Phys. B **30**, 365 (1997).
[16] F. Folkmann, K. O. Groeneveld, R. Mann, G. Nolte, S. Schumann, and R. Spohr, Z. Phys. A **275**, 229 (1975).
[17] F. Bloch, Z. Phys. **81**, 363 (1933).
[18] J. Lindhard and A. H. Sørensen, Phys. Rev. A **53**, 2443 (1996).
[19] M. Jung, H. Rothard, B. Gervais, J. P. Grandin, A. Clouvas, and R. Wünsch, Phys. Rev. A **54**, 4153 (1996).
[20] *CRC Handbook of Chemistry and Physics*, edited by D. R. Lide and H. P. R. Frederikse (CRC Press, New York, 1997).